



Imaging and tracking of tumor extracellular vesicles to unravel the progression of ovarian carcinoma using fluorescent membrane probes

Ting Wang^{a,b,1}, Qingyuan Liu^{a,b,1}, Xingya Chen^{a,b}, Yueyue Zhao^{a,b}, Yan Chen^{a,b}, Rui Wang^{a,b}, Fabiao Yu^{a,b,*}, Yanlong Xing^{a,b,*}

^a Key Laboratory of Hainan Trauma and Disaster Rescue, The First Affiliated Hospital of Hainan Medical University, Hainan Medical University, Haikou 571199, China

^b Engineering Research Center for Hainan Bio-Smart Materials and Bio-Medical Devices, Key Laboratory of Emergency and Trauma, Ministry of Education, Key Laboratory of Hainan Functional Materials and Molecular Imaging, College of Emergency and Trauma, Hainan Medical University, Haikou 571199, China

ARTICLE INFO

Keywords:

Extracellular vesicles
Ovarian carcinoma
Homing effect
Fluorescence imaging
Membrane probes

ABSTRACT

Tumor extracellular vesicles (EVs) exert vital role in mediating intercellular communication. Investigation on the function of EVs will contribute to understanding of EV pathophysiology in cancer development. However, direct visualizing the behavior of EVs *in vivo* still faces challenges. In this study, we develop fluorescently labelled EVs derived from ovarian carcinoma (OC-EVs) utilizing lipid dye and protein-based membrane probes, which are investigated in living cells and mice models by high-resolution fluorescence imaging and ultrasonic imaging. Both membrane probes exhibit high labelling efficiency of EVs and good compatibility *in vivo*. The rapid internalization of individual OC-EVs by different single living cells are monitored, together with the complex and bidirectional exchange of EVs between normal and cancer cells. Furthermore, the enrichment of OC-EVs in ovary is recorded, indicating the homing targeting capability of EVs. For more precise observation of the homing process, *in vivo* ultrasonic imaging and fluorescence imaging are performed to evaluate the rapidly growing ovarian tumor after administrating OC-EVs. The results show that OC-EVs can accelerate tumor growth and promote the metastasis of primary tumors in mice, which provides valuable information in understanding the development of ovarian carcinoma and pursuing potential solution for improved treatment.

1. Introduction

Extracellular vesicles (EVs) are lipid bilayer vesicles that are secreted into the extracellular environment by all known organisms [1,2]. EVs have been extensively investigated owing to the vital role in transporting bioactive cargos and mediating the intercellular communication to regulate various biological processes [3–6]. Therefore, knowledge of EV biology and application has gained wide interest and grown rapidly [7–10]. Typically, EVs have been employed as potential targets to study the mechanism of cargo transport of cancer cells and their influence on tumor development [11,12]. However, investigation on EVs' function faces challenges, for instance, lack of powerful live imaging tools, efficient labelling strategies or suitable animal models [13–15]. In addition, EVs preserve heterogeneity due to complex biogenesis, which put hurdles in EV biology and pathology research including cancer [16–18].

Recent years, it has been reported that a multitude of noninvasive

imaging methods has been investigated to explore the spatio-temporal dynamics of nanoparticles *in vitro* and *in vivo* [19–21], by combining with advanced labeling strategies [22,23]. For instance, fluorescently labelled EVs have been visualized at cellular level or *in vivo* [24,25], using lipid membrane dyes such as PKH67, DiR [26], Membright dyes [14], or using fluorescent EVs secreted from genetically encoded cells [15,27,28]. However, the visualized tracking EVs biodistribution and the assessment on EVs' function in tumor development has only been sparsely investigated due to the above-mentioned challenges, which limits the insights into EVs pathophysiology, especially in single vesicle level [29].

Among the various cancer types, ovarian carcinoma is the gynecologic malignancy with the highest case-to-fatality ratio, putting threaten on female health worldwide [30]. It has been reported that EVs exert crucial function in shuttle molecules to receipt cells and influence cancer development [11,31]. In particular, the homing targeting ability of EVs

* Corresponding authors at: Key Laboratory of Hainan Trauma and Disaster Rescue, The First Affiliated Hospital of Hainan Medical University, Hainan Medical University, Haikou 571199, China.

E-mail addresses: yufabiao@hainmc.edu.cn (F. Yu), xingyanlong@hainmc.edu.cn (Y. Xing).

¹ These authors contributed equally to this work.

contributes to cancer growth and metastases [32]. However, there is still a lack of direct evidence on the function of ovarian cancer EVs in affecting tumor progression.

Herein, we employ two labelling strategies to obtain fluorescently labelled ovarian cancer derived EVs (OC-EVs) for exploring their role in the development of ovarian carcinoma (Scheme 1). In one aspect, lipid membrane probes including PKH67 and Mem560 (short for MemGlow560) are used to stain EVs, which exhibit high labelling efficiency and compatibility. In another aspect, EVs with fluorescent protein membrane labels are obtained from genetically encoding cells. Based on the two kinds of fluorescent EVs, the interaction of single EVs with individual cells, as well as the bi-directional EV exchange between normal ovarian cells and ovarian cancer cells are recorded, providing *in vitro* evidence of the homing potential of EVs to homologous cells. *In vivo* monitoring the distribution of EVs unveil the hepatic-leading metabolism process. Meanwhile, the enrichment of EVs in brain suggests the capability of EVs in crossing brain-blood-barrier (BBB) and the accumulation in ovary also demonstrated the homing ability of OC-EVs. Finally, by applying genetically modified OC-EVs to *in situ* ovarian tumor-bearing mice, the rapid growth of tumor is monitored and recorded with fluorescence and ultrasonic imaging techniques, which evidently demonstrate the homing ability of EVs in accelerating tumor growth. Altogether, based on lipid and fluorescent protein membrane probes, we successfully demonstrate the function of tumor EVs in promoting ovarian cancer, thereby offering valuable information for addressing other open questions in EV biology and promoting the development of EV therapeutics.

2. Materials and methods

2.1. Isolation of EVs

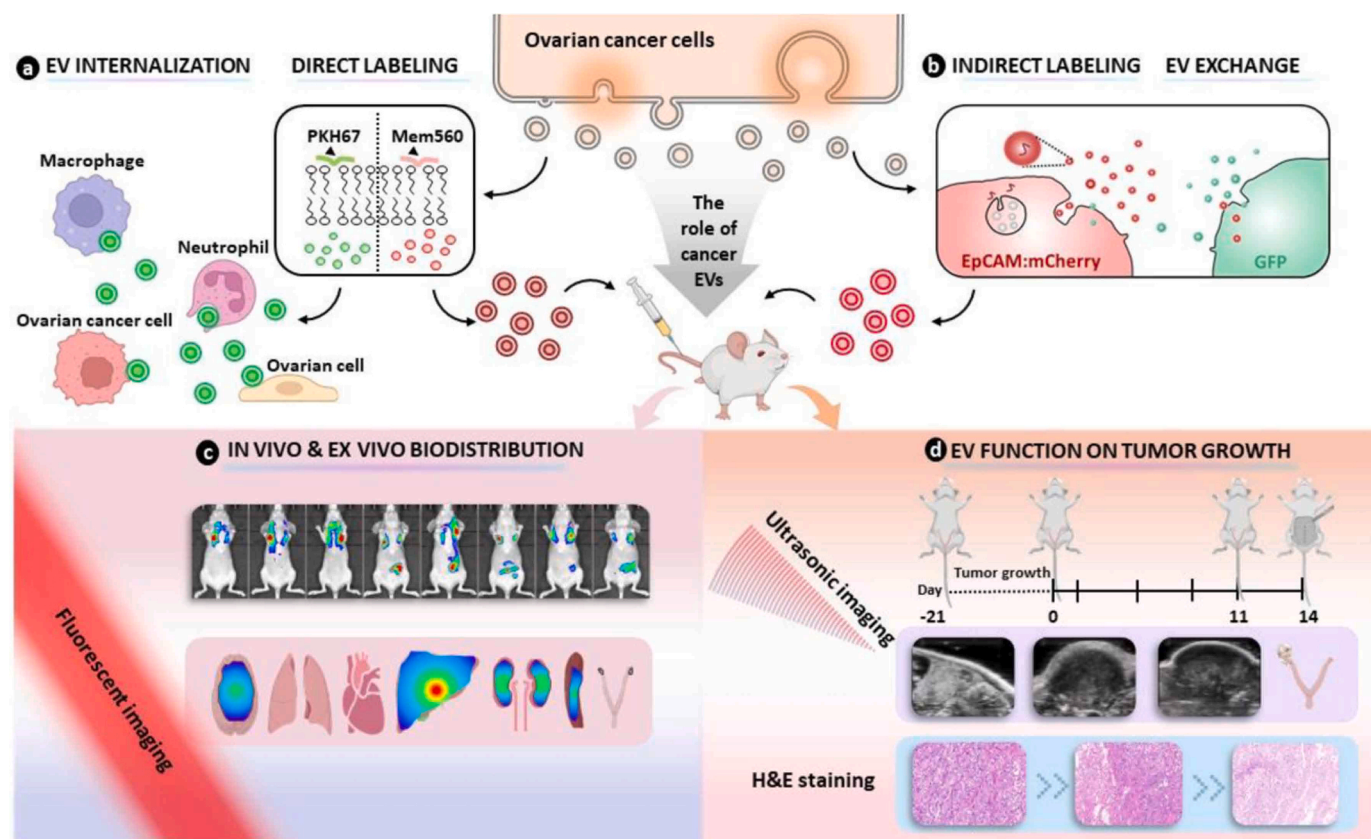
EVs were obtained following the recommendations of the International Society of Extracellular Vesicles. Typically, EVs were extracted by differential centrifugation at 4 °C (Eppendorf 5810 R centrifuge) following the steps of 1) 300 × g, 10 min. 2) 2000 × g, 10 min. 3) 10,000 × g, 30 min. 4) Filtration of culture supernatant by 0.22 μm filter (100 K, Millex, Millipore). 5) 5000 × g centrifugation for 30 min. 6) 100,000 × g ultracentrifugation (Hitachi CS150GXL) for 70 min to obtain EV precipitate.

2.2. Labeling of EVs using PKH67 and Mem560

EV precipitation was suspended with 0.5 mL Diluent C. After adding 5 μL PKH67 dye (Sigma, 200 nM, final concentration) or Mem560 (Cytoskeleton, 200 nM, final concentration) solution, the mixture was incubated at r.t. in dark for 5 min. Then the mixture was ultracentrifuged at 100,000 × g for 70 min to obtain precipitate. After resuspension in 8 mL EV-free medium and centrifugation, PKH67/Mem560-labeled EVs was obtained.

2.3. Construction of fluorescent protein expressed cell lines

Cells was seeded into 6-well plates and cultured for 12 h. According to the MOI (multiplicity of infection) of cells and virus titer, the amount of corresponding virus (overexpressing GFP or EpCAM:mCherry) was added (virus volume = (MOI × cell number)/virus titer). After culturing for 48 h, the infection efficiency was monitored until the fusion degree reached about 80 %. Then the cells were cultured in 1 μg / mL puromycin complete medium and changed every 2 days until complete



Scheme 1. Schematic illustration of imaging and tracking of tumor extracellular vesicles to unravel the progression of ovarian carcinoma using fluorescent membrane probes.

infection was observed under fluorescence microscope. Then the cells were cultured under reduced concentration of puromycin.

2.4. Ultrasonic imaging of *in situ* ovarian carcinoma-bearing mice

All the animal experiments were approved by the Institutional Animal Care and Use Committee and Ethics Committee of Hainan Medical University (Approval number: HYLL-2022-302). Female nude mice bearing *in situ* ovarian carcinoma were randomly divided into model group, PBS treated group and experimental group for further experiment following the plan displayed in Fig. 6a. The size, volume and morphological changes of ovarian tumors nude mice were measured by ultrasonic imaging device (Vevo3100LT system).

2.5. Fluorescence imaging of healthy mice and tumor-bearing mice models

Female BALB/c healthy nude mice were randomly divided into control and experimental groups. Mice were anaesthetized with isoflurane throughout the experiment. In the control group, only Mem560 dye (200 nM) was administrated *via* intraperitoneal or tail vein injection, while OC-EVs-Mem560 (1×10^9 particles/mL) were used in the experimental group. *In vivo* and *ex vivo* imaging was performed using IVIS Lumina XR III system ($\lambda_{ex} / \lambda_{em} = 555/570$ nm, acquisition time 0.1 s). For mice bearing *in situ* xenotransplanted ovarian tumor, *in vivo* and *ex vivo* imaging was performed after injection of OC-EVs-mCherry ($\lambda_{ex} / \lambda_{em} = 587/610$ nm, acquisition time 0.1 s).

3. Results and discussion

3.1. Membrane lipid dyes label EVs with high compatibility

To obtain fluorescent OC-EVs, we employed PKH67 and Mem560 as

the lipid membrane binding probes. PKH 67 is the conventional lipid dye which is commonly used for tracing of cell vesicles [33], while Mem560 is a new type of membrane probe to label cell membrane and EVs (Fig. 1a) [34]. Before labelling, OC-EVs were characterized by transmission electron microscopy (TEM), which displayed typical cup-shape structure with an average size of 100 nm (Fig. 1b, i and enlarged image in orange box). Additionally, western-blot analysis (WB) of OC-EVs showcased obvious bands of CD63, TSG101 and EpCAM antibodies (left, Fig. 1c), which demonstrated the successful isolation of OC-EVs. Nanoparticle tracking analysis (NTA) revealed that OC-EVs had an average diameter of 144.7 nm and a peak diameter of 133.0 nm (Fig. 1d, i). These characterization results confirmed the successful isolation of EVs [3]. OC-EVs were then labeled with Mem560 (OC-EVs-Mem560) and PKH67 (OC-EVs-PKH67) dyes and analyzed by TEM, WB and NTA. The TEM results of OC-EVs-Mem560 (Fig. 1b ii and the enlarged image in green box) and OC-EVs-PKH67 (Fig. 1b iii and the enlarged image in blue box), the similar WB bands of them with those of OC-EVs (middle and right, Fig. 1c), together with the NTA results (Fig. 1d, ii & iii) confirmed that the morphology, content and size of lipid dye labeled EVs were not significantly affected after labelling, which demonstrated the biocompatibility of lipid membrane dyes.

3.2. Genetically encoded reporters can specifically and brightly label cells and EVs

In addition, we utilized a genetically approach to label cells and obtain fluorescent protein labeled EVs by secretion. As illustrated in Fig. 2a, ovarian cells were transfected with GFP to enable releasing of EVs expressing GFP (HO23-EVs-GFP, upper panel), while ovarian cancer cells were incubated with EpCAM-overexpressing mCherry to stably express red fluorescence and secret EVs (OC-EVs-mCherry, lower panel). Live-cell confocal microscopy of HO23-GFP cell revealed numerous

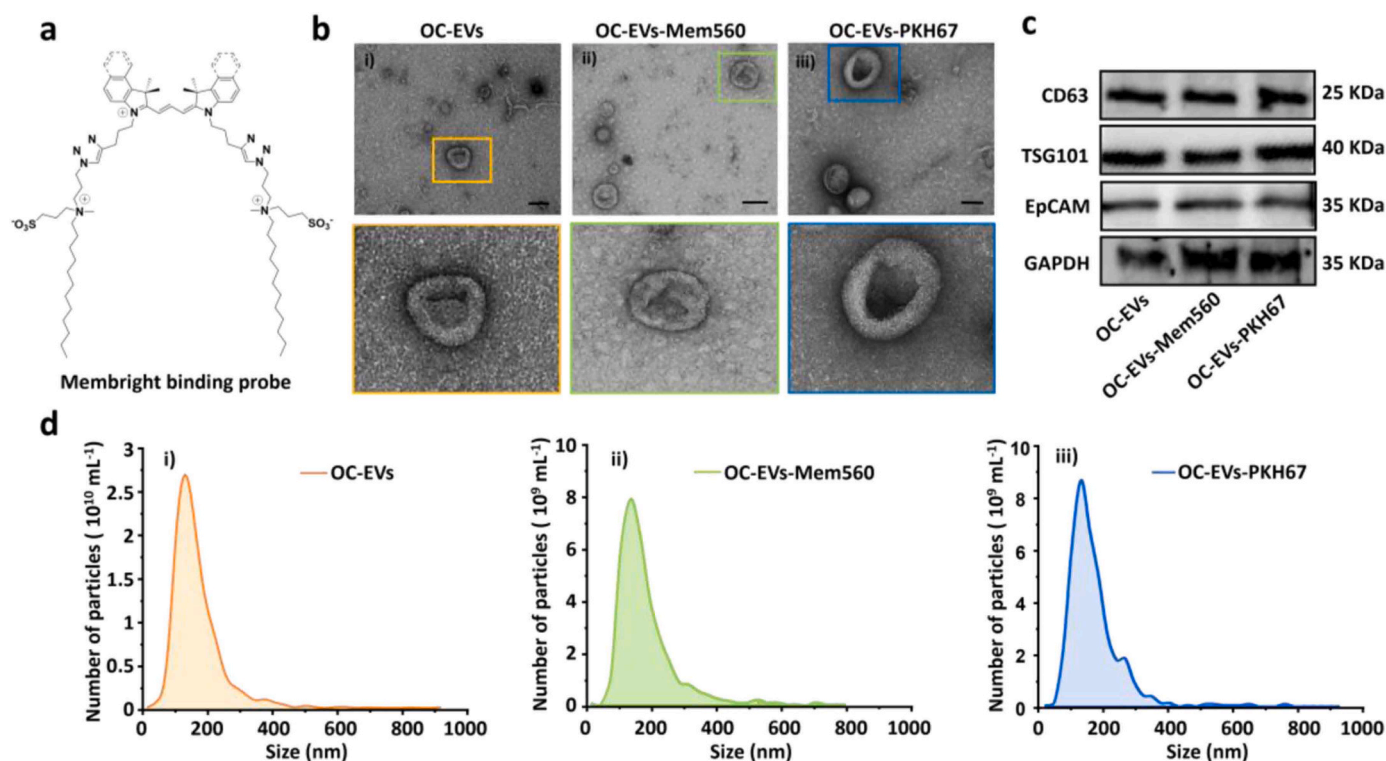


Fig. 1. Characterization of the OC-EVs before and after fluorescent dye labelling. (a) Molecular structure of the membrane binding probe MemBright. (b) TEM of OC-EVs, OC-EVs-Mem560 and OC-EVs-PKH67. Enlarged images of single EVs displayed in the bottom showed the respective boxed area of images in the top. Scale bars, 100 nm. (c) Western blot analysis of EVs with anti-CD63, anti-TSG101, anti-EpCAM, using GAPDH as loading control. (d) NTA results of i) OC-EVs ii) OC-EVs-Mem560 (average diameter of 155.7 nm with peak diameter of 129.5 nm) and iii) OC-EVs-PKH67 (average diameter of 153.7 nm and peak diameter of 144.6 nm) showing the concentration (y axis) and diameter (x axis).

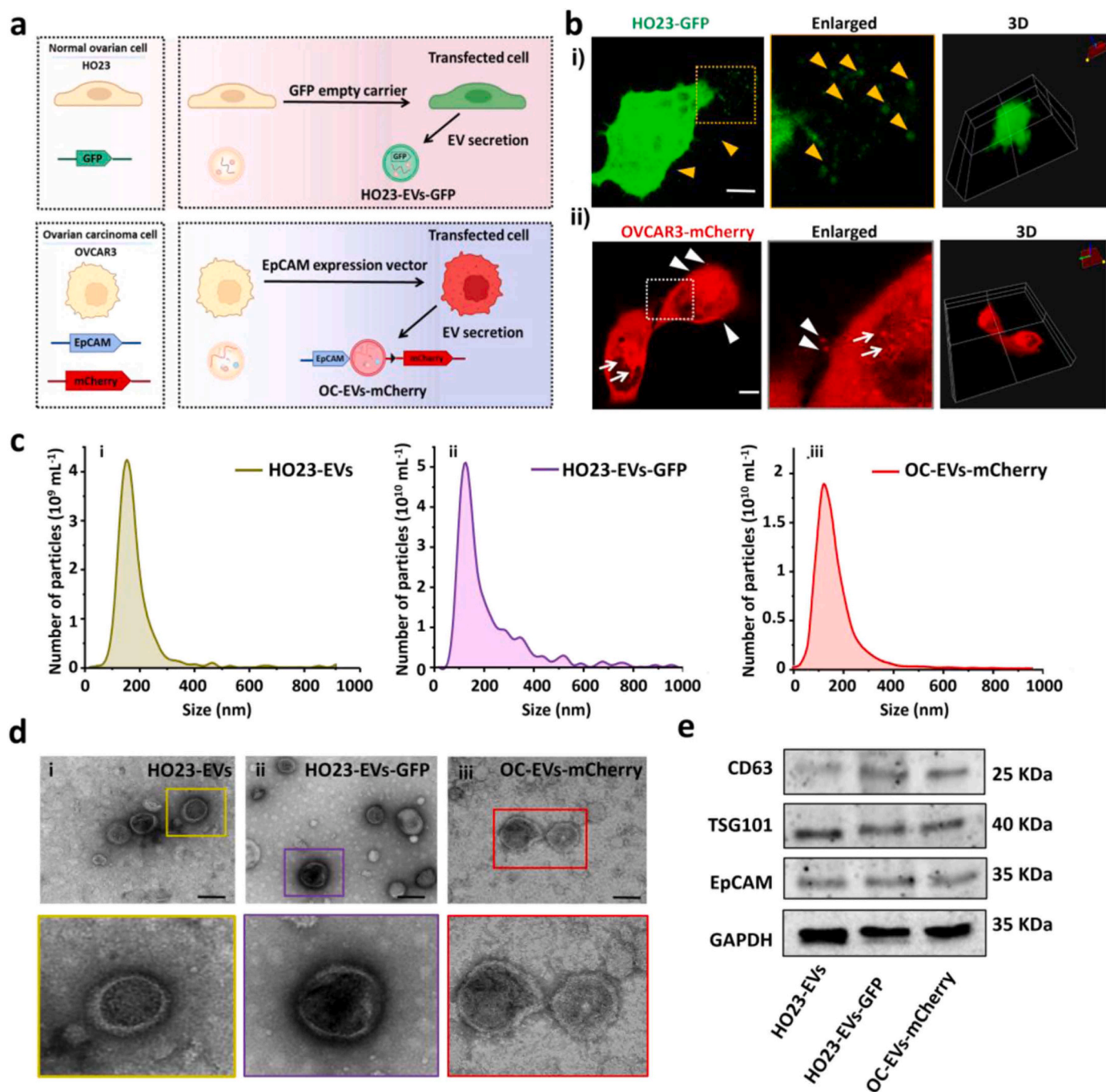


Fig. 2. (a) Schematic diagram of cell membrane labelling with GFP (HO23 cells, top) or mCherry (EpCAM overexpression, OVCAR3 cells, bottom) and the secretion of transfected EVs. (b) Live cell confocal fluorescence imaging of i) HO23-GFP cells and ii) OVCAR3-mCherry cells, the enlarged images of boxes area and the 3D imaging of cells. Scale bars, 5 μm . (c) NTA results of EVs derived from i) HO23 cells ii) HO23-GFP cells and iii) OVCAR3-mCherry cells. (d) TEM of HO23-EVs, HO23-EVs-GFP and OC-EVs-mCherry. Scale bars, 100 nm. (e) Western blot analysis of three types of EVs using CD63, TSG101 and EpCAM antibodies, using GAPDH as loading control.

GFP-positive deposits surrounding the cell, suggesting the release of vesicles by HO23-GFP cells (Fig. 2b, i, left and enlarged yellow boxed region images, yellow arrow heads, and Fig. S1a i, ii). Additionally, the GFP-positive deposits exhibited various sizes, indicating that GFP labeled multiple vesicle-like structures (Fig. 2b, i, right panel 3D image). The live-cell fluorescence imaging of OVCAR3-mCherry cells showcased that mCherry uniformly labeled the plasma membrane and displayed budlike structure on their surface (Fig. 2b, ii, left and enlarged white boxed region images, white arrows, 3D image) and red puncta in the extracellular region (white arrow heads) (Fig. S1a iii). Furthermore, the

particles released by HO23-GFP cells and OVCAR3-mCherry cells were collected and characterized. The NTA results of HO-EVs-GFP (average and peak diameter of 152.1 nm and 140.5 nm, respectively) and OC-EVs-mCherry (average and peak diameter of 169.9 nm and 147.5 nm, respectively) (Fig. 2c, ii and iii) were comparable with the size distribution of HO23-EVs (average diameter of 158.3 nm and peak diameter of 158.3 nm) (Fig. 2c, i). Additionally, the TEM images (Fig. 2d) and WB results (Fig. 2e) suggested the successful isolation of HO-EVs, and transfection of both HO23 cells and OVCAR3 cells, as well as the possibility of obtaining membrane protein labelled EVs with GFP or

mCherry reporters.

3.3. High-resolution tracking of individual EVs interaction with diverse cells

To understand how tumor EVs target specific cell types [14], we investigated the interaction between OC-EVs and different cells including macrophages, neutrophils, ovarian cells and ovarian cancer cells. Firstly, after labeling macrophages with Mem560 (20 nM) and Hoechst, OC-EVs-PKH67 were added and cocultured. The fluorescent images in Fig. 3a revealed that OC-EVs-PKH67 penetrated the cell

membrane and accumulated in the cytoplasm, exhibiting time dependent trend in 60 min (Fig. 3b). Following, the interaction between individual OC-EVs and single cells were tracked. As showcased in Fig. 3c and Movie S1, single OC-EVs-PKH67 could be rapidly taken up by a live macrophage cell within 44 s. The 3D imaging results clearly showed the internalized green vesicle inside the red cell membrane (Fig. 3d and Fig. S2a, b). These findings indicated the interaction between tumor EVs and macrophages, which would promote tumor growth and invasion [35]. Since PKH67 dye was reported to affect the observation of EVs [14], we then utilized OC-EVs-Mem560 to interact with GFP-expressing macrophage. As displayed in Fig. 3e and Fig. S1c, macrophage-GFP

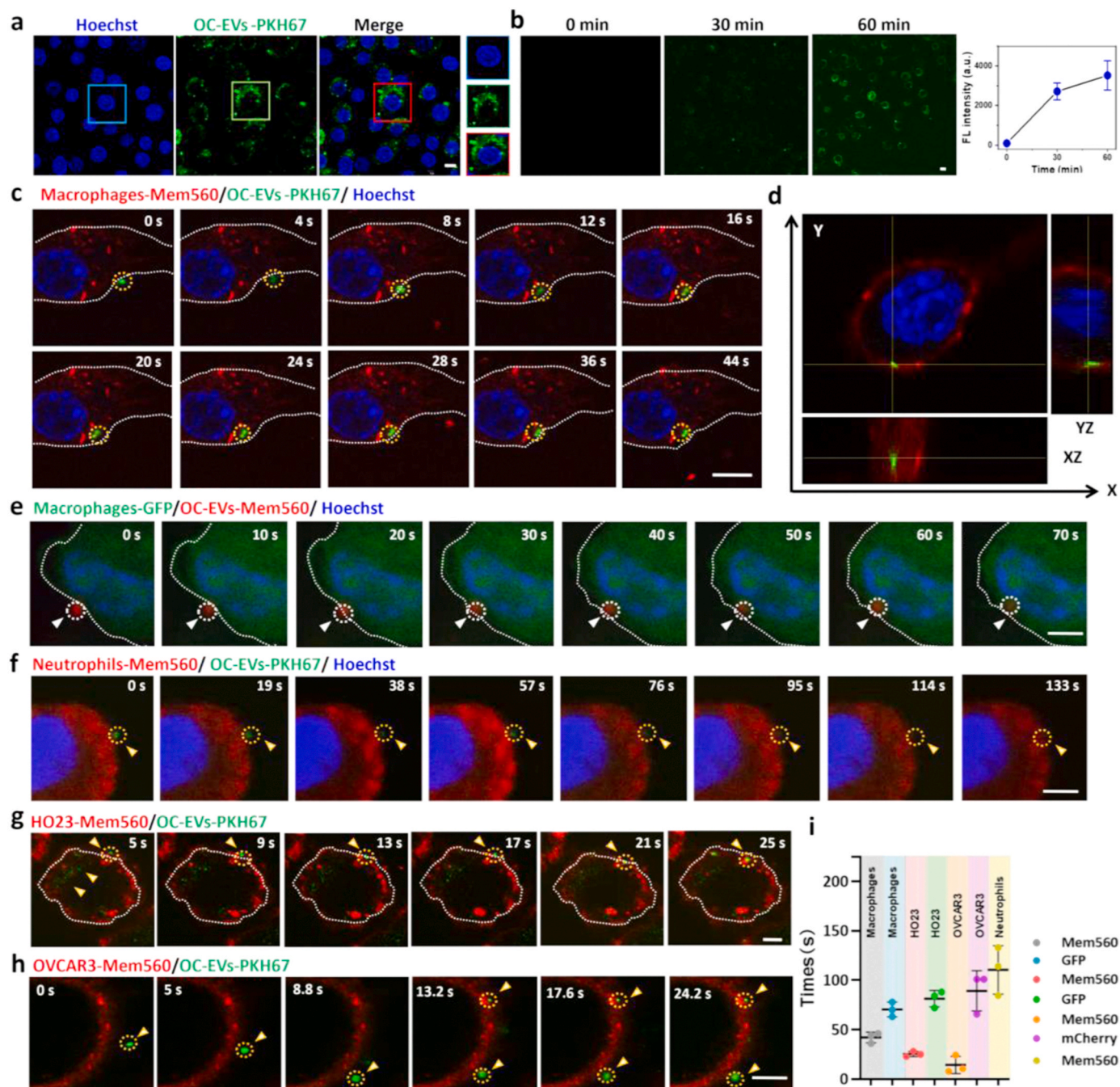


Fig. 3. (a) Fluorescence imaging of macrophages (RAW264.7) cocultured with OC-EVs-PKH67. Figures show the blue, green, merge channels and figure inset of individual cells. (b) Fluorescence imaging of OC-EVs-PKH67 internalized in macrophages at different time and the quantitative result. (c) Dynamic tracking of the interaction between macrophage-Mem560 and OC-EVs-PKH67. (d) The XZ and YZ display of 3D imaging of the cell in Fig. c. Time-dependent fluorescence imaging of the interaction between (e) Macrophage-GFP and OC-EVs-Mem560 (f)-(g) showed interaction of OC-EVs-PKH67 with neutrophil-Mem560, HO23-Mem560 and OVCAR3-Mem560. (i) Comparison of different internalization time of OC-EVs by various cells. Scale bars, 5 μ m.

could internalize individual OC-EVs-Mem560 in 70 s (Movie S2), conforming the efficiency of using both PKH67 and Mem560 labeling to monitor OC-EVs. Neutrophils were also utilized to interact with OC-EVs-PKH67, which could uptake EVs in around 133 s (Fig. 3f and Fig. S3). Additionally, the interaction between OC-EVs and HO23 cells or OVCAR3 cells were investigated, with HO23 cells exhibiting rapid uptake of OC-EVs within 25 s (Fig. 3g, Fig. S4 and Movie S3). In the case of OVCAR3 cells, OC-EVs-PKH67 moved towards OVCAR3 cell in 24.2 seconds and attached to the cell membrane (Fig. 3h), mapping of z-line sequential images and the XZ and YZ display of 3D imaging revealed that the observed OC-EVs-PKH67 embedded in the cell membrane (Fig. S5 and Movie S4). These results demonstrated the homing effect of tumor EVs to parental cells of the same origin, while exhibiting much severe tendency to normal cells. Interestingly, after incubating Mem560-labeled OVCAR3 cell in exosome-free medium, we noticed that the labeled OVCAR3 could shed some vesicle-like red particles from filopodia (Fig. S6, Movie S5), suggesting the biogenesis of EVs via inheriting membrane contents from parental cell [2].

Supplementary material related to this article can be found online at [doi:10.1016/j.snb.2024.135975](https://doi.org/10.1016/j.snb.2024.135975).

Following, we compared the time required for diverse cells to uptake OC-EVs. As illustrated in Fig. 3i, macrophage-Mem560 took around 43 s

to internalize OC-EVs, while macrophage-GFP consumed about 70 s. HO23-Mem560 could uptake OC-EVs within an average period of 29 s, while HO23-GFP need around 84 s. Similarly, OVCAR3 cells could arrest OC-EVs within about 23 s, however, OVCAR3-mCherry required 88 s. In the case of neutrophils, about 109 s was needed to finish the internalization. These results indicated that these cells were involved in the transferring of tumor EVs, with macrophages, HO23 and OVCAR3 cells capturing OC-EVs faster than neutrophil. Also, lipid dye labeled cells consumed shorter time than lentivirus-infected cells. Importantly, the internalization of OC-EVs by ovarian cells provided *in vitro* evidence of the homing characteristics of EVs to homologous cells.

3.4. EVs release from transfected cells and exchange between cell populations

Using a complementary strategy, we constructed fluorescent protein labelled cells to obtain EVs for investigating the one-way and dynamic exchange of EVs between different cell populations [13]. As displayed in Fig. 4a, we inoculated OVCAR3-mCherry cells and HO23-GFP cells in the two sides of a culture insert in one petri dish. After removing the insert, the co-incubation of the two types of cells were monitored (Fig. 4a and Fig. S7a, i). EVs were released and the existence of single

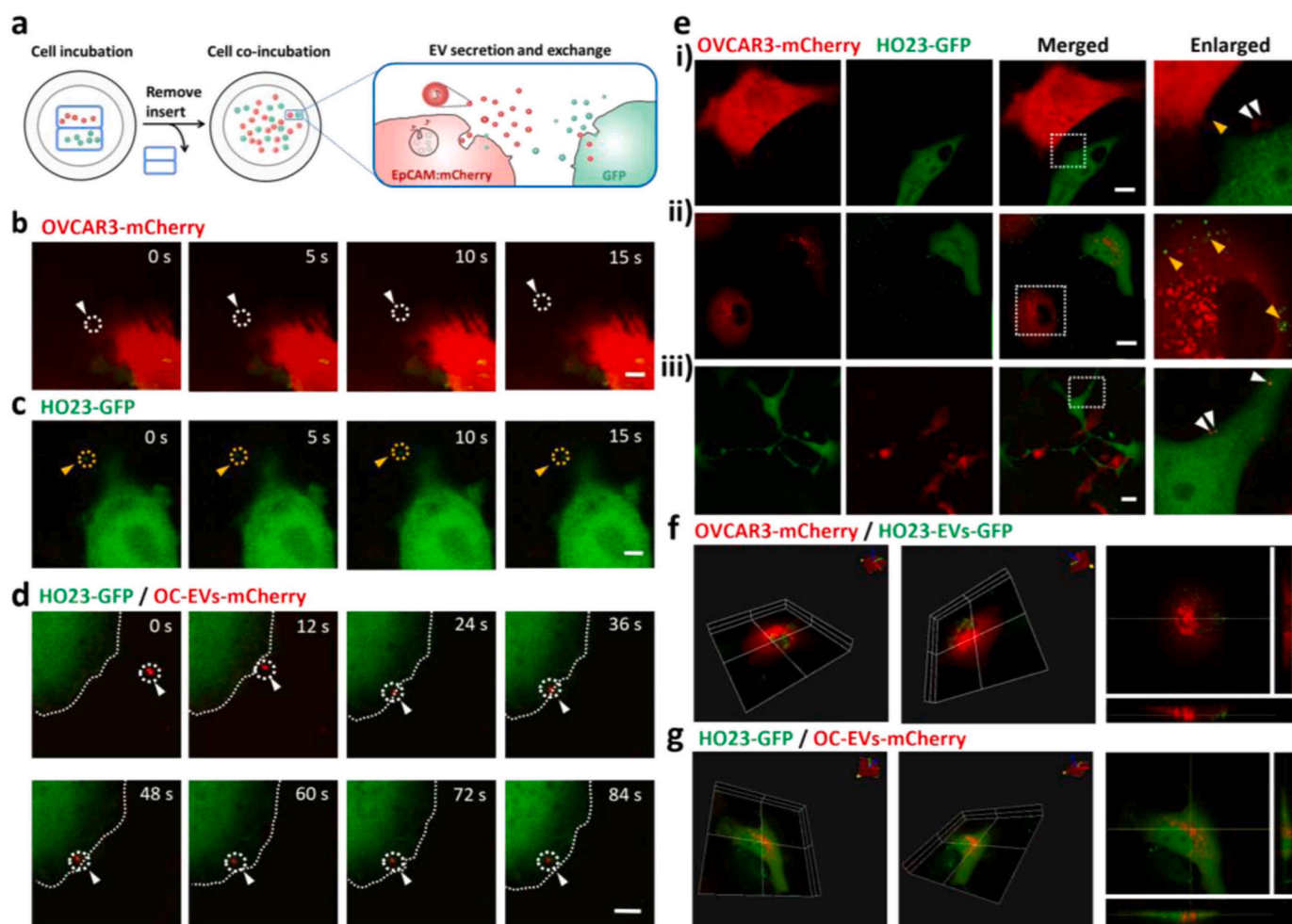


Fig. 4. (a) Schematic illustration of co-incubation of OVCAR3-mCherry cells and HO23-GFP cells. Time-lapsed confocal imaging of (b) OVCAR3-mCherry cells and (c) HO23-GFP cells. Scale bars, 5 μ m. (d) Time-lapsed imaging of the internalization of OC-EVs-mCherry by a HO23-GFP cell within 84 s with time interval of 12 s. Scale bars, 5 μ m. (e) Live-cell imaging of EVs exchange and uptake between OVCAR3-mCherry and HO23-GFP cells. Magnification of boxes in merged panels are shown in enlarged images. i) EVs released from two cell lines were observed in surrounding regions (white and yellow arrowhead). ii) EVs secreted from HO23-GFP cell were observed inside the OVCAR3-mCherry cell (yellow arrowhead). iii) EVs secreted from OVCAR3-mCherry cell were found inside the HO23-GFP cell (white arrowhead). Scale bars, 20 μ m. (f) and (g) The 3D imaging of OVCAR3-mCherry cell and internalized HO23-EVs-GFP, and HO23-GFP cell with captured OC-EVs-mCherry.

EVs surrounding individual cells was recorded (Fig. 4b and 4c). Time-lapsed imaging of OC-EVs-mCherry-exposed HO23-GFP cell displayed the movement of EVs towards recipient cell and final uptake within 84 s (Fig. 4d). This result demonstrated the effectiveness in using the protein membrane reporters to differentiate recipient cells from tumor EVs. During co-incubation, both cell types were also found to extend and release vesicles, which were then taken up by the other cell type (Fig. 4e and Fig. S7a, ii-iv). The 3D imaging of a typical OVCAR3-mCherry cell obviously showcased the internalized green vesicles released from HO23-GFP cells (Fig. 4f and Fig. S7b). Similar phenomenon was observed in a HO23-GFP cell with captured red vesicles (Fig. 4g and Fig. S7c). These data collectively demonstrated the biological process of ovarian cancer cells and normal ovarian cells, including EVs' release, intercellular communication of one-way delivery and bi-directional exchange between cell populations.

3.5. *In vivo* distribution and toxicity of lipid dye labelled and genetically encoded OC-EVs

Based on the *in vitro* experiment results, we then addressed the distribution and toxicity of lipid dye and fluorescent protein labelled OC-EVs *in vivo* using 6–8-week-old healthy female BALB/c nude mice. As displayed in Fig. 5a, i), the mice were pretreated 24 h before experiment and injected with OC-EVs-Mem560 through intraperitoneal (I. P.) or tail vein (I. V.) injection, with Mem560 dye as control. Then *in vivo* imaging of mice in each group was performed at different time point till 7 d. Afterwards, the mice were sacrificed to obtain organs for fluorescence imaging. The studied mice were randomly divided into four groups: Group I, I. P. injection of Mem560 dye; Group II, I. P. injection of OC-EVs-Mem560; Group III, I. V. injection of Mem560 dye; Group IV, I. V. injection of OC-EVs-Mem560. *In vivo* imaging was performed at different time points of 1 h, 2 h, 6 h, 12 h, 24 h, 48 h, 72 h, and 7 d after injection. In the control groups, fluorescence signals were observed mainly at liver in nude mice 1 h postinjection and peaked at 12 h (Fig. S8a, c). Then the fluorescence intensity gradually decreased over time and was neglectable on 7 d, indicating the hepatic-leading metabolism process. In contrast, for the OC-EVs-Mem560 groups, fluorescence was detected at different parts of the mice 1 h postinjection and could be detected until 7 d (Fig. S8b, d).

After *in vivo* imaging, the nude mice were sacrificed at each time point to obtain the organs (brain, lung, heart, liver, kidney, spleen and ovary) for *ex vivo* imaging. As showcased in Fig. 5b, the Mem560 dye was mainly accumulated in liver (i and iii) [36] and peaked at 12 h postinjection, then metabolized until 7 d. In the experimental groups, the injected OC-EVs-Mem560 exhibited similar organ distribution and time-dependent metabolism, but with distinguishable signal on 7 d (Fig. 5b, ii and iv). Fluorescence signal was also observed in kidney, indicating the renal metabolism process. The obvious fluorescence observed in brain showed the BBB-penetrating capability of OC-EVs-Mem560, while the fluorescence in ovary demonstrated their homing effect. Interestingly, we observed that OC-EVs-Mem560 accumulated more in the brain *via* I. V. injection than I. P. injection, mainly attributed to the rapid transfer through blood flow. The *ex vivo* imaging of organs offered accurate distribution and quantification of administrated vesicles, in accordance with the *in vivo* imaging results displayed in Fig. S8. Besides, the quantitative results of the fluorescence imaging of organs (Fig. 5c and 5d) again confirmed that liver was the main organ responsible for EV metabolism, following with kidney.

OC-EVs-mCherry was also investigated following the experiment schedule in Fig. 5a (ii). As shown in Fig. 5e, EVs were mainly enriched in the liver, following by brain, kidney, spleen, lung and ovary, displaying time-dependent distribution characteristics. Fluorescence signal was peaked at around 24 h and gradually decreased over time, but was still obvious until 7 d. The imaging of organs and quantitative results (Fig. 5f and Fig. 5g) again demonstrated the hepatic and renal clearance of EVs *in vivo*. Additionally, the longer metabolism time of protein labeled

EVs in mice (highest at 24 h in liver) than lipid dye group (highest at 12 h in liver) was in accordance with the cell imaging results. Altogether, we documented that both types of membrane probes could label OC-EVs with high biocompatibility for *in vivo* imaging. Importantly, the enrichment of OC-EVs in ovary evidently confirmed the homing targeting capability of EVs.

3.6. Investigation on the effects of OC-EVs on metastatic growth of tumor cells *in vivo*

Tumor EVs modulate cancer progression and influence the metastasis of primary tumors [37–40]. We then established *in situ* xenotransplanted ovarian tumor bearing nude mice model (left ovary) and utilized OC-EVs-mCherry to evaluate their *in vivo* function following the plan in Fig. 6a. *In situ* ovarian cancer mice models were randomly divided into experimental group and PBS group and treated with OC-EVs-mCherry and PBS separately *via* I. V. injection. Afterwards, the sizes of ovarian tumors were monitored by ultrasonic imaging. The body weight (BW) and abdominal circumference (AC) were also measured. When the tumor grew to around 1 mm³, the mice were sacrificed, and the organs were observed *ex vivo* by photographing and fluorescence imaging.

Representative mice photos were displayed in Fig. 6b. On day 0, compared to the healthy mouse in control group, a bulge was visible on the lower left back of the model group. The ultrasonic imaging in Fig. 6c indicated the sizes of the ovaries of normal mice (control group, approx. 1.5 mm × 1.5 mm × 1.5 mm), with no obvious blood signals. However, in the model group, a cystic mass (approx. 9.3 mm × 6.2 mm × 7.1 mm) could be observed in the left ovary, with typical solid tumor characteristics of partially unclear boundary, uneven echo and rich blood flow signals. Afterwards, mice in control and model group were sacrificed to obtain the main organs for further measurement. As showcased in Fig. 6d, the size of the ovary of representative control group was 1.76 mm × 2.07 mm × 2.01 mm. The left ovary of model mouse exhibited irregular cauliflower like structure (Fig. 6d model group), with hard texture and larger size (5.70 mm × 9.65 mm × 7.07 mm) than the control group. Furthermore, the H & E staining of the main organs (brain, liver and left ovary) of control and model groups were performed. As shown in Fig. 6e, compared to the normal structure in control group, the brain tissue in the model group showed obvious nucleus shrinkage. Together with the pathological characteristics in liver and ovarian tissues, the successful establishment of *in situ* ovarian cancer mice model was confirmed.

Following, the *in situ* xenograft OVCAR3-tumor bearing nude mice were randomly divided into experimental group and PBS group, which were administrated OC-EVs-mCherry or PBS separately, following the experimental plan in Fig. 6a. During the treatment process, we monitored the ovary changes by ultrasonic imaging (Fig. 6c and Fig. S9) until the tumor grew to around 0.9 mm³ on day 11 (Fig. S9b). On day 14, obvious enlarged bulges were observed on the lower left back part of the PBS and OC-EVs-mCherry group (dotted black circles, Fig. 6b). Then the mice in both groups were sacrificed to obtain main organs for further measurement. As shown in Fig. 6d, the left ovaries of PBS and OC-EVs-mCherry-treated groups both exhibited irregular cauliflower like structure, hard texture, and large size (4.46 mm × 6.80 mm × 6.78 mm and 9.73 mm × 11.77 mm × 8.18 mm, respectively). Furthermore, H & E staining of the main organs (brain, liver and ovary) of both groups indicated that the PBS-treated group deteriorated worse than the model group, suggesting the progression of tumor (Fig. 6e). Compared with the PBS group, the deterioration of tissues in the OC-EVs-mCherry-treated group was much severe, indicating the pathological function of OC-EVs in accelerating tumor progression. Both groups exhibited gradually increased AC (Fig. S10a) and decreased BW, with the OC-EVs-mCherry group much severe (Fig. S10b), owing to the development of ovarian tumor. The changes of ovarian volume and tumor growth speed of two groups were also evaluated based on the ultrasonic imaging

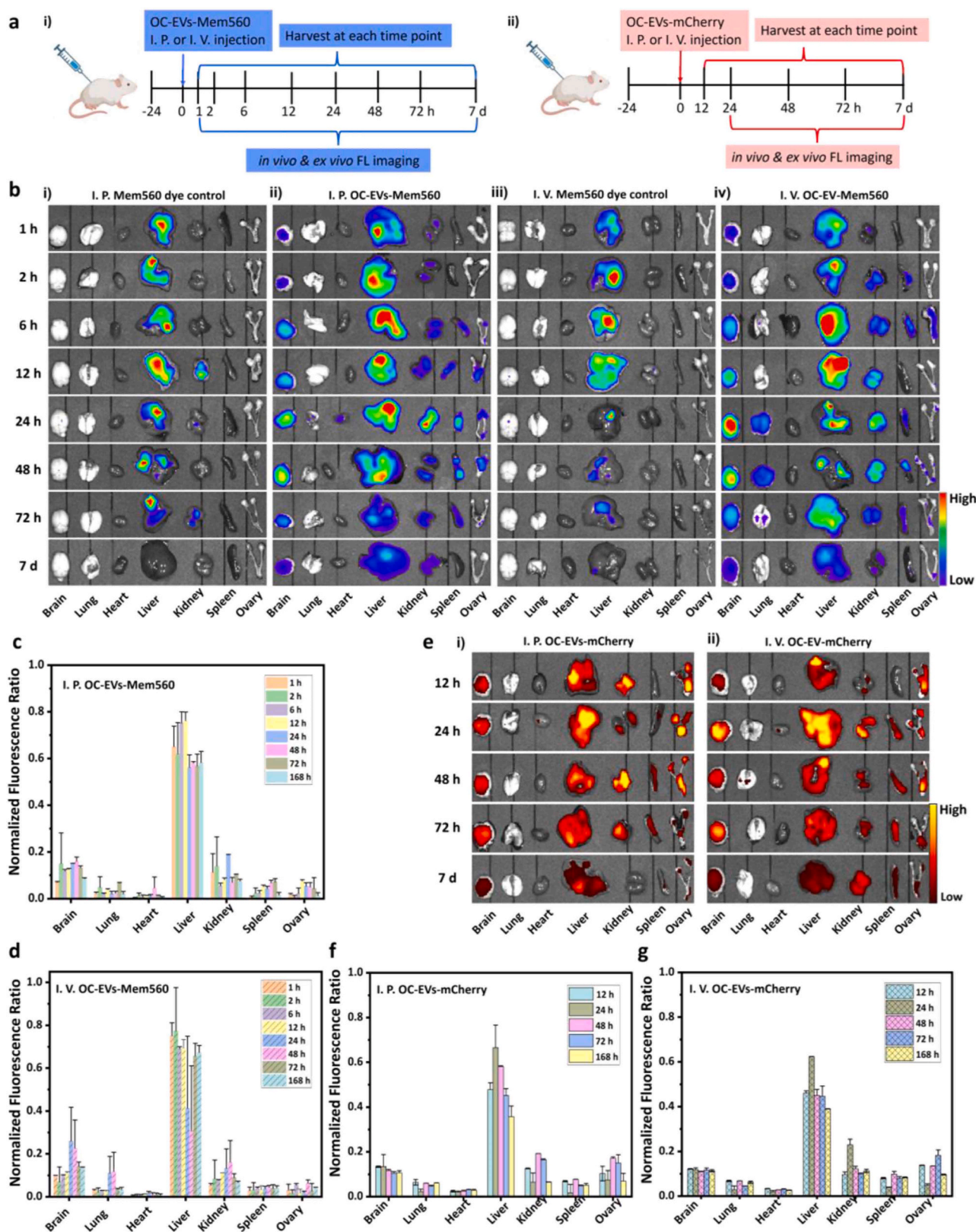


Fig. 5. *In vivo* and *ex vivo* imaging of OC-EVs. (a) Bioimaging plan after using i) OC-EVs-Mem560 and ii) OC-EVs-mCherry via I. P. or I. V. injection. (b) *Ex vivo* fluorescence (FL) imaging of organs (brain, lung, heart, liver, kidney, spleen and ovary) harvested from the mice treated with i) Mem560 dye and ii) OC-EVs-Mem560, I. P. injection. iii) Mem560 dye and iv) OC-EVs-Mem560, I. V. injection. (c) and (d) are quantification results of images displayed in Fig. b ii) and iv), analyzed by recording the photons/second/steradian (ph/s/sr) of each organ and normalized to that of the injected dose based on the fluorescence intensity. Data shown as mean ($n = 3$). (e) *Ex vivo* imaging of main organs harvested from the mice treated with OC-EVs-mCherry via i) I. P. injection or ii) I. V. injection. (f) and (g) quantification of imaging results displayed in Fig. e. Data shown as mean ($n = 3$).

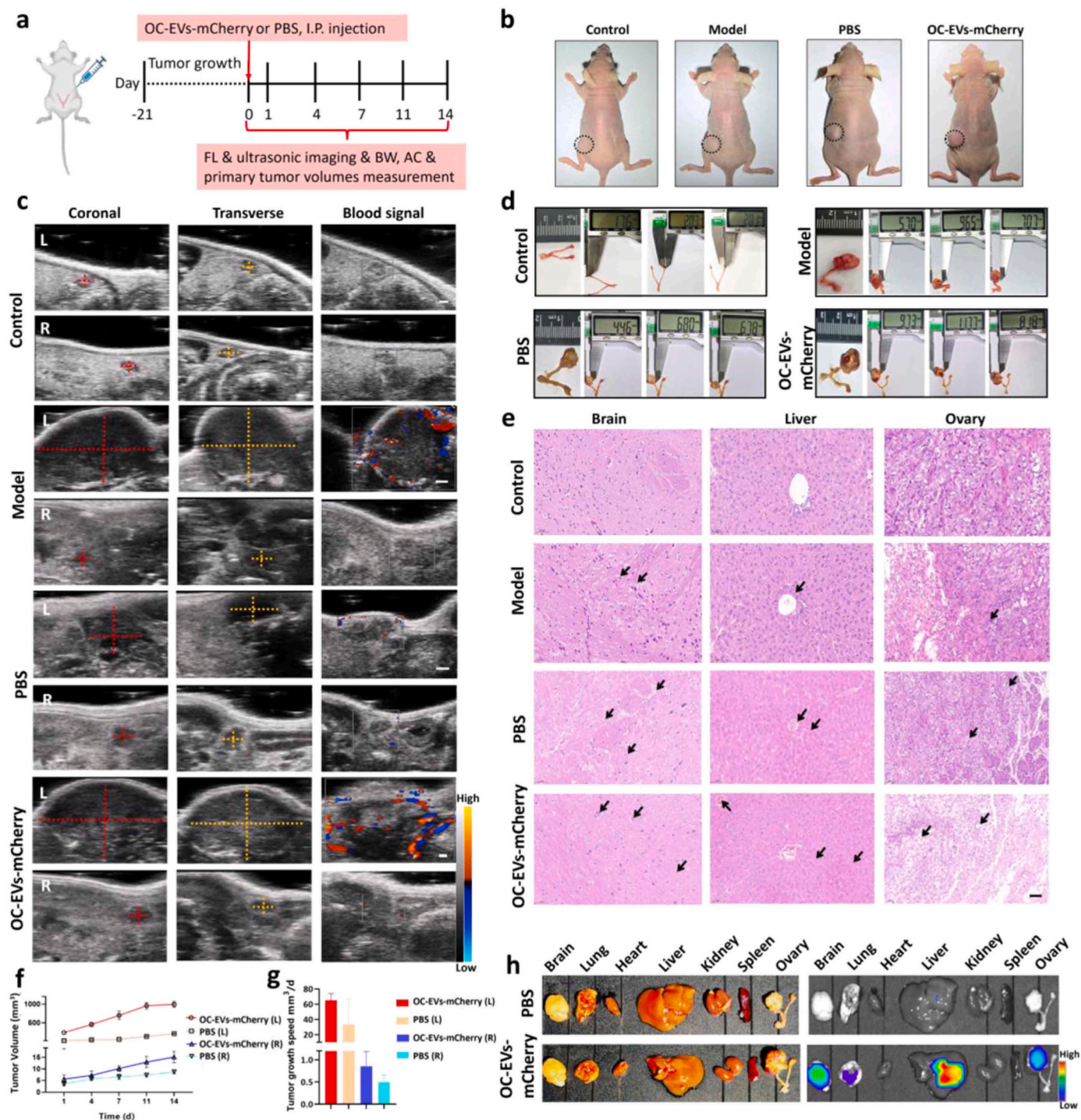


Fig. 6. Investigation on the function of OC-EVs on tumor progression in mice models. (a) Schematic illustration of the experimental plan. (b) Photographs of the representative mice of the control (day 0), model (day 0), PBS (day 14) and OC-EVs-mCherry (day 14) groups. (c) Ultrasonic imaging of the mice displayed in Fig. b, images showed left (L) and right (R) ovaries from coronal, transverse views, and the blood signal. Scale bars, 1 mm. (d) Photographs of the reproductive system of the mice in Fig. b. The size of left ovary was measured by a vernier caliper. (e) H&E-stained slices of the brain, liver and ovary of the mice in Fig. b. Scale bars, 50 μ m. (f) Ovarian volumes (mm^3) of the left (L) and right (R) ovaries of the mice treated with PBS and OC-EVs-mCherry, measured by ultrasonic imaging (day1-day 11) and vernier caliper (day 14). (g) Ovarian tumor growth speed calculated from Fig. f and displayed in mm^3/d . (h) Photographs (left) and fluorescence imaging (right) of organs harvested from the mice treated with PBS and OC-EVs-mCherry.

results on day 0–11 (Fig. 6c and Fig. S9b) and the measurement on day 14 (Fig. 6d). It could be seen from Fig. 6f and Fig. 6g, the tumor volume and growth speed of OC-EVs-mCherry-treated group increased faster upon time than the PBS-treated group (Figs. 6f and 6g, OC-EVs-mCherry (L) & PBS (L)), suggesting the promotion function of OC-EVs-mCherry on ovarian tumor. To our surprise, the right ovary of the OC-EVs-

mCherry-treated group (Figs. 6f and 6g, OC-EVs-mCherry (R)) also exhibited obvious increment compared to the PBS group (Fig. 6f and 6g, PBS (R)), probably attributing to the influence of OC-EVs.

Judging from the photographs of main organs of both groups, apart from ovary, no obvious abnormalities in the other organs was observed under naked eyes (Fig. 6h left panel). As displayed in Fig. 6h (right

panel), evident fluorescence was observed in the organs (brain, lung, liver and ovary) of OC-EVs-mCherry-treated group, with strong fluorescence in ovary, again demonstrating evident homing capability of OC-EVs and their function in promoting tumor growth.

4. Conclusions

In this study, we employed two types of membrane probes to obtain fluorescently labelled EVs and successfully visualized OC-EVs *in vitro* and *in vivo*. Based on the direct labeling of EVs by lipophilic membrane probes (PKH67 and Mem560), we recorded the single vesicle internalization by various cells (including macrophage, neutrophil, ovarian cell and ovarian cancer cell). Using indirect labeling of vesicles by harvesting EVs from lentivirus (GFP and EpCAM:mCherry) transfected cells, we observed the one-way delivery and bidirectional exchange of EVs between normal ovarian cells and cancer cells. These data indicated the liability of cancer EVs to interact with cells of the same origin, mainly attributing to the homing characteristics of EVs. By administrating fluorescently labelled OC-EVs into mice models, the hepatic and renal clearance process, as well as the homing effect of EVs were unveiled. Furthermore, by injecting OC-EVs into xenotransplanted ovarian tumor bearing nude mice, the function of OC-EVs in promoting tumor growth was verified. In general, our findings supported the EV-mediated intercellular communication, which were complex, multi-directional, far-reaching, and homing. We also confirmed the metabolism routes of EVs *in vivo* and the essential function of EVs in accelerating tumor development. Future studies would focus on the underlying molecular mechanism dominated in EVs influence on tumor progression, which would provide potential targets for tumor treatment.

CRediT authorship contribution statement

Ting Wang: Writing – original draft, Project administration, Methodology. **Qingyuan Liu:** Validation, Software, Data curation. **Xingya Chen:** Visualization, Software, Data curation. **Yueyue Zhao:** Validation, Software, Data curation. **Yan Chen:** Software, Data curation. **Rui Wang:** Writing – review & editing. **Fabiao Yu:** Supervision, Funding acquisition, Conceptualization. **Yanlong Xing:** Writing – review & editing, Supervision, Resources, Methodology, Funding acquisition, Conceptualization.

Declaration of Competing Interest

The authors declare the following financial interests/personal relationships which may be considered as potential competing interests: Fabiao Yu, Yanlong Xing reports financial support was provided by National Natural Science Foundation of China. Yanlong Xing, Rui Wang reports financial support was provided by Hainan Provincial Natural Science Foundation of China. Yanlong Xing reports financial support was provided by Nanhai Young-Talent Program of Hainan. Fabiao Yu reports financial support was provided by Hainan Province Clinical Medical Center (2021). Fabiao Yu reports financial support was provided by Project for Functional Materials and Molecular Imaging Science Innovation Group of Hainan Medical University (2022). If there are other authors, they declare that they have no known competing financial interests or personal relationships that could have appeared to influence the work reported in this paper.

Data availability

Data will be made available on request.

Acknowledgements

This work was supported by National Natural Science Foundation of China (Nos. 82360417 and 22264013), Hainan Provincial Natural

Science Foundation of China (ZDYF2024SHFZ131 and ZDYF2024SHFZ104), Nanhai Young-Talent Program of Hainan (20202018), Project for Functional Materials and Molecular Imaging Science Innovation Group of Hainan Medical University (2022). The illustrations (Scheme 1, Fig. 5a & Fig. 6a) were created with the help of BioRender.com.

Appendix A. Supporting information

Supplementary data associated with this article can be found in the online version at [doi:10.1016/j.snb.2024.135975](https://doi.org/10.1016/j.snb.2024.135975).

References

- [1] G. van Niel, G. D'Angelo, G. Raposo, Shedding light on the cell biology of extracellular vesicles, *Nat. Rev. Mol. Cell Biol.* 19 (2018) 213–228, <https://doi.org/10.1038/nrm.2017.125>.
- [2] M. Colombo, G. Raposo, C. Théry, Biogenesis, secretion, and intercellular interactions of exosomes and other extracellular vesicles, *Annu. Rev. Cell Dev. Biol.* 30 (2014) 255–289, <https://doi.org/10.1146/annurev-cellbio-101512-122326>.
- [3] H. Shao, H. Im, C.M. Castro, X. Breakefield, R. Weissleder, H. Lee, New technologies for analysis of extracellular vesicles, *Chem. Rev.* 118 (2018) 1917–1950, <https://doi.org/10.1021/acs.chemrev.7b00534>.
- [4] Y. Xing, Z. Cheng, R. Wang, C. Lv, T.D. James, F. Yu, Analysis of extracellular vesicles as emerging theranostic nanoplatforms, *Coord. Chem. Rev.* 424 (2020) 213506, <https://doi.org/10.1016/j.ccr.2020.213506>.
- [5] M. Tkach, C. Théry, Communication by extracellular vesicles: where we are and where we need to go, *Cell* 164 (2016) 1226–1232, <https://doi.org/10.1016/j.cell.2016.01.043>.
- [6] M. Mathieu, L. Martin-Jaular, G. Lavieu, C. Théry, Specificities of secretion and uptake of exosomes and other extracellular vesicles for cell-to-cell communication, *Nat. Cell Biol.* 21 (2019) 9–17, <https://doi.org/10.1038/s41556-018-0250-9>.
- [7] H. Feng, S. Min, Y. Huang, Z. Gan, C. Liang, W.-D. Li, Y. Chen, Concentric gradient nanoplasmonic sensors for detecting tumor-derived extracellular vesicles, *Sens. Actuators B Chem.* 400 (2024) 134899, <https://doi.org/10.1016/j.snb.2023.134899>.
- [8] J. Kim, J. Park, S. Ahn, S. Park, H. Yu, J. Yu, D. Kim, J.-Y. Lim, K.-A. Hyun, W.-G. Koh, H.-I. Jung, On-demand delivery of therapeutic extracellular vesicles by encapsulating in monodispersed photodegradable hydrogel microparticles using a droplet microfluidic device, *Sens. Actuators B Chem.* 394 (2023) 134396, <https://doi.org/10.1016/j.snb.2023.134396>.
- [9] C. Ducrot, S. Loiseau, C. Wong, E. Madec, J. Volatron, M. Piffoux, Hybrid extracellular vesicles for drug delivery, *Cancer Lett.* 558 (2023) 216107, <https://doi.org/10.1016/j.canlet.2023.216107>.
- [10] J. Chen, J. Guo, M. Hu, Y. Wang, F. Hua, H.-M. Meng, S. Jin, Accurate and portable tumor exosomes detection based on manganese dioxide and aptamer-functionalized fluorescent microspheres mediated dual-mode lateral flow assay, *Sens. Actuators B Chem.* 409 (2024) 135614, <https://doi.org/10.1016/j.snb.2024.135614>.
- [11] K. Lopez, S.W.T. Lai, E.J. Lopez Gonzalez, R.G. Dávila, S.C. Shuck, Extracellular vesicles: a dive into their role in the tumor microenvironment and cancer progression, *Front. Cell Dev. Biol.* 11 (2023) 1154576, <https://doi.org/10.3389/fcell.2023.1154576>.
- [12] R. Kalluri, V.S. LeBleu, The biology, function, and biomedical applications of exosomes, *Science* 367 (2020) eaau6977, <https://doi.org/10.1126/science.aau6977>.
- [13] C.P. Lai, E.Y. Kim, C.E. Badr, R. Weissleder, T.R. Mempel, B.A. Tannous, X. O. Breakefield, Visualization and tracking of tumour extracellular vesicle delivery and RNA translation using multiplexed reporters, *Nat. Commun.* 6 (2015) 7029, <https://doi.org/10.1038/ncomms8029>.
- [14] V. Hyenne, S. Ghoroghi, M. Collot, J. Bons, G. Follain, S. Harlepp, B. Mary, J. Bauer, L. Mercier, I. Busnelli, O. Lefebvre, N. Fekonja, M.J. Garcia-Leon, P. Machado, F. Delalande, A.A. López, S.G. Silva, F.J. Verweij, G. van Niel, F. Djouad, H. Peinado, C. Carapito, A.S. Klymchenko, J.G. Goetz, Studying the fate of tumor extracellular vesicles at high spatiotemporal resolution using the zebrafish embryo, *Dev. Cell* 48 (2019) 554–572, <https://doi.org/10.1016/j.devcel.2019.01.014>, e557.
- [15] B.H. Sung, A. von Lersner, J. Guerrero, E.S. Krystofiak, D. Inman, R. Pelletier, A. Zijlstra, S.M. Ponik, A.M. Weaver, A live cell reporter of exosome secretion and uptake reveals pathfinding behavior of migrating cells, *Nat. Commun.* 11 (2020) 2092, <https://doi.org/10.1038/s41467-020-15747-2>.
- [16] T. Wang, Y. Xing, Z. Cheng, F. Yu, Analysis of single extracellular vesicles for biomedical applications with especial emphasis on cancer investigations, *Trends Anal. Chem.* 152 (2022) 116604, <https://doi.org/10.1016/j.trac.2022.116604>.
- [17] G. Corso, W. Heusermann, D. Trojer, A. Görgens, E. Steib, J. Voshol, A. Graff, C. Genoud, Y. Lee, J. Hean, J.Z. Nordin, O.P.B. Wiklander, S. El Andaloussi, N. Meisner-Kober, Systematic characterization of extracellular vesicle sorting domains and quantification at the single molecule – single vesicle level by fluorescence correlation spectroscopy and single particle imaging, *J. Extracell. Vesicles* 8 (2019) 1663043, <https://doi.org/10.1080/20013078.2019.1663043>.
- [18] C. Han, M. Kang, H. Kang, J. Yi, M. Lim, Y. Kwon, J. Park, Characterization of extracellular vesicle and virus-like particles by single vesicle tetraspanin analysis,

- Sens. Actuators B: Chem. 382 (2023) 133547, <https://doi.org/10.1016/j.snb.2023.133547>.
- [19] F.J. Verweij, L. Balaj, C.M. Boulanger, D.R.F. Carter, E.B. Compeer, G. D'Angelo, S. El Andaloussi, J.G. Goetz, J.C. Gross, V. Hyenne, E.-M. Krämer-Albers, C.P. Lai, X. Loyer, A. Marki, S. Momma, E.N.M. Nolte-t Hoen, D.M. Pegtel, H. Peinado, G. Raposo, K. Rilla, H. Tahara, C. Théry, M.E. van Royen, R.E. Vandenbroucke, A. M. Wehman, K. Witwer, Z. Wu, R. Wubbolts, G. van Niel, The power of imaging to understand extracellular vesicle biology in vivo, *Nat. Methods* 18 (2021) 1013–1026, <https://doi.org/10.1038/s41592-021-01206-3>.
- [20] H. Chen, H. Wang, Y. Wei, M. Hu, B. Dong, H. Fang, Q. Chen, Super-resolution imaging reveals the subcellular distribution of dextran at the nanoscale in living cells, *Chin. Chem. Lett.* 33 (2022) 1865–1869, <https://doi.org/10.1016/j.ccllet.2021.10.025>.
- [21] X. Song, R. Wang, J. Gao, X. Han, J. Jin, C. Lv, F. Yu, Construction of a biotin-targeting drug delivery system and its near-infrared theranostic fluorescent probe for real-time image-guided therapy of lung cancer, *Chin. Chem. Lett.* 33 (2022) 1567–1571, <https://doi.org/10.1016/j.ccllet.2021.08.111>.
- [22] M.S. Panagopoulou, A.W. Wark, D.J.S. Birch, C.D. Gregory, Phenotypic analysis of extracellular vesicles: a review on the applications of fluorescence, *J. Extracell. Vesicles* 9 (2020) 1710020, <https://doi.org/10.1080/20013078.2019.1710020>.
- [23] Y.-S. Chen, C. Chen, C.P.-K. Lai, G.-B. Lee, Isolation and digital counting of extracellular vesicles from blood via membrane-integrated microfluidics, *Sens. Actuators B: Chem.* 358 (2022) 131473, <https://doi.org/10.1016/j.snb.2022.131473>.
- [24] F. Pucci, C. Garris, C.P. Lai, A. Newton, C. Pfirsche, C. Engblom, D. Alvarez, M. Sprachman, C. Evavold, A. Magnuson, U.H. von Andrian, K. Glatz, X. O. Breakefield, T.R. Mempel, R. Weissleder, M.J. Pittet, SCS macrophages suppress melanoma by restricting tumor-derived vesicle–B cell interactions, *Science* 352 (2016) 242–246, <https://doi.org/10.1126/science.aaf1328>.
- [25] Y. He, Y. Xing, T. Jiang, J. Wang, S. Sang, H. Rong, F. Yu, Fluorescence labeling of extracellular vesicles for diverse bio-applications in vitro and in vivo, *Chem. Commun.* 59 (2023) 6609–6626, <https://doi.org/10.1039/D3CC00998J>.
- [26] E. Lázaro-Ibáñez, F.N. Faruqu, A.F. Saleh, A.M. Silva, J. Tzu-Wen Wang, J. Rak, K. T. Al-Jamal, N. Dekker, Selection of fluorescent, bioluminescent, and radioactive tracers to accurately reflect extracellular vesicle biodistribution in vivo, *ACS Nano* 15 (2021) 3212–3227, <https://doi.org/10.1021/acsnano.0c09873>.
- [27] A. Zomer, C. Maynard, Frederik J. Verweij, A. Kamerians, R. Schäfer, E. Beerling, Raymond M. Schiffelers, E. de Wit, J. Berenguer, Saskia Inge J. Ellenbroek, T. Wurdinger, Dirk M. Pegtel, J. van Rheenen, In vivo imaging reveals extracellular vesicle-mediated phenocopying of metastatic behavior, *Cell* 161 (2015) 1046–1057, <https://doi.org/10.1016/j.cell.2015.04.042>.
- [28] F.J. Verweij, C. Revenu, G. Arras, F. Dingli, D. Loew, D.M. Pegtel, G. Follain, G. Allio, J.G. Goetz, P. Zimmermann, P. Herbolom, F. Del Bene, G. Raposo, G. van Niel, Live tracking of inter-organ communication by endogenous exosomes in vivo, *Dev. Cell* 48 (2019) 573–589, <https://doi.org/10.1016/j.devcel.2019.01.004>, e574.
- [29] G. Bordanaba-Florit, F. Royo, S.G. Kruglik, J.M. Falcón-Pérez, Using single-vesicle technologies to unravel the heterogeneity of extracellular vesicles, *Nat. Protoc.* 16 (2021) 3163–3185, <https://doi.org/10.1038/s41596-021-00551-z>.
- [30] R.L. Siegel, K.D. Miller, H.E. Fuchs, A. Jemal, *Cancer statistics, 2022*, *CA Cancer J. Clin.* 72 (2022) 7–33, <https://doi.org/10.3322/caac.21708>.
- [31] M. Nawaz, F. Fatima, I. Nazarenko, K. Ekström, I. Murtaza, M. Anees, A. Sultan, L. Neder, G. Camussi, H. Valadi, J.A. Squire, T. Kislinger, Extracellular vesicles in ovarian cancer: applications to tumor biology, immunotherapy and biomarker discovery, *Expert Rev. Proteom.* 13 (2016) 395–409, <https://doi.org/10.1586/14789450.2016.1165613>.
- [32] L. Blavier, R. Nakata, P. Neviani, K. Sharma, H. Shimada, A. Benedicto, I. Matei, D. Lyden, Y.A. DeClerck, The capture of extracellular vesicles endogenously released by xenotransplanted tumours induces an inflammatory reaction in the premetastatic niche, *J. Extracell. Vesicles* 12 (2023) 12326, <https://doi.org/10.1002/jev2.12326>.
- [33] Á.M. Bellmunt, L. López-Puerto, J. Lorente, D. Closa, Involvement of extracellular vesicles in the macrophage-tumor cell communication in head and neck squamous cell carcinoma 14 (2019) e0224710, <https://doi.org/10.1371/journal.pone.0224710>.
- [34] M. Collot, P. Ashokkumar, H. Anton, E. Boutant, O. Faklaris, T. Galli, Y. Mély, L. Danglot, A.S. Klymchenko, MemBright: a family of fluorescent membrane probes for advanced cellular imaging and neuroscience, *Cell Chem. Biol.* 26 (2019) 600–614, <https://doi.org/10.1016/j.chembiol.2019.01.009>, e607.
- [35] A. Chow, W. Zhou, L. Liu, M.Y. Fong, J. Champer, D. Van Haute, A.R. Chin, X. Ren, B.G. Gugu, Z. Meng, W. Huang, V. Ngo, M. Kortylewski, S.E. Wang, Macrophage immunomodulation by breast cancer-derived exosomes requires Toll-like receptor 2-mediated activation of NF- κ B, *Sci. Rep.* 4 (2014) 5750, <https://doi.org/10.1038/srep05750>.
- [36] O.P.B. Wiklander, J.Z. Nordin, A. O'Loughlin, Y. Gustafsson, G. Corso, I. Mäger, P. Vader, Y. Lee, H. Sork, Y. Seow, N. Heldring, L. Alvarez-Erviti, C.I.E. Smith, K. Le Blanc, P. Macchiarini, P. Jungebluth, M.J.A. Wood, S.E.L. Andaloussi, Extracellular vesicle in vivo biodistribution is determined by cell source, route of administration and targeting, *J. Extracell. Vesicles* 4 (2015) 26316, <https://doi.org/10.3402/jev.v4.26316>.
- [37] V. Hyenne, O. Lefebvre, J.G. Goetz, Going live with tumor exosomes and microvesicles, *Cell Adhes. Migr.* 11 (2017) 173–186, <https://doi.org/10.1080/19336918.2016.1276694>.
- [38] H. Peinado, H. Zhang, I.R. Matei, B. Costa-Silva, A. Hoshino, G. Rodrigues, B. Psaila, R.N. Kaplan, J.F. Bromberg, Y. Kang, M.J. Bissell, T.R. Cox, A.J. Giaccia, J.T. Erler, S. Hiratsuka, C.M. Ghajar, D. Lyden, Pre-metastatic niches: organ-specific homes for metastases, *Nat. Rev. Cancer* 17 (2017) 302–317, <https://doi.org/10.1038/nrc.2017.6>.
- [39] L.M. Desrochers, M.A. Antonyak, R.A. Cerione, Extracellular vesicles: satellites of information transfer in cancer and stem cell biology, *Dev. Cell* 37 (2016) 301–309, <https://doi.org/10.1016/j.devcel.2016.04.019>.
- [40] M. Wang, W. Cai, A.-J. Yang, C.-Y. Wang, C.-L. Zhang, W. Liu, X.-F. Xie, Y.-Y. Gong, Y.-Y. Zhao, W.-C. Wu, Q. Zhou, C.-Y. Zhao, J.-F. Dong, M. Li, Gastric cancer cell-derived extracellular vesicles disrupt endothelial integrity and promote metastasis, *Cancer Lett.* 545 (2022) 215827, <https://doi.org/10.1016/j.canlet.2022.215827>.

Ting Wang received her Master's degree from Hainan Medical University in 2022. She then worked as an attending physician at resident physician at the Guangzhou General Hospital. Her research focuses on fluorescence imaging of extracellular vesicles (EVs) and single EV analysis.

Qingyuan Liu received his Bachelor's degree from Xixiang Medical University in 2022. He is now a Master student in Hainan Medical University. His research focuses on analysis of tumor extracellular vesicles using fluorescence imaging and Surface-enhanced Raman spectroscopy.

Xingya Chen received her Bachelor of Medicine degree from Harbin Medical University in 2016. She then worked as a laboratory physician in the Third Hospital Affiliated of Qiqihar Medical College, and was enrolled in Hainan Medical College for her master's degree in 2021. Her research focuses on the phenotypic changes of extracellular vesicles using microfluidic chip technology combined with surface-enhanced Raman spectroscopy to achieve early diagnosis of tumours.

Yueyue Zhao received her Bachelor's degree from Hainan Medical University in 2021. She is working on her Master's degree from the same university. Her research focuses on multiplexed profiling of single extracellular vesicles using fluorescence imaging for diagnosis of various malignant tumors.

Yan Chen received her Master's degree from Hainan Medical University in 2021. She is now pursuing her doctoral degree and doing research on tumor and pathology using molecular biology and ultrasonic imaging techniques.

Rui Wang received his Ph.D. degree from Hanyang University, Korea in 2018. Afterwards, he has been working as associated professor at Hainan Medical University. His current research focuses on development of novel clinical diagnostic and therapeutic approaches towards bacteria using fluorescent or Raman techniques.

Fabiao Yu received his Ph.D. degree from Dalian University of Technology and Dalian Institute of Chemical Physics, Chinese Academy of Sciences in 2013. After four years' work at Yantai Institute of Coastal Zone Research, Chinese Academy of Sciences as an associate professor, he joined Hainan Medical University from 2018 as a full professor. His research interests focus on molecular diagnosis of tropical disease, multi-modal visual surgery navigation, and point-of-care testing (POCT) technology.

Yanlong Xing received her Ph.D. degree from Technical University of Berlin (Jan. 2017) and was a doctoral researcher in the Swiss Federal Institute of Technology (2013–2015) and Postdoctoral Research Fellow in ISAS Berlin (2017–2018). She is now an associate professor at Hainan Medical University. Her current research focuses on extracellular vesicle-based liquid biopsy and microfluidic-assisted detection of biomolecules using fluorescent and Raman microscopy.